Advances in Science and Technology Research Journal, 2026, 20(1), 301–317 https://doi.org/10.12913/22998624/210455 ISSN 2299-8624, License CC-BY 4.0 Received: 2025.07.14 Accepted: 2025.09.25 Published: 2025.11.21

# Physics-informed neural network for identifying the hysteresis model of the vacuum-packed particles torsional damper

Mateusz Żurawski<sup>1\*</sup>, Dominik Rodak<sup>1</sup>, Robert Zalewski<sup>1</sup>

- <sup>1</sup> Faculty of Automotive and Construction Machinery Engineering, Warsaw University of Technology, ul. Narbutta 84, 02-524, Warsaw, Poland
- \* Corresponding author's e-mail: Mateusz.Zurawski@pw.edu.pl

### **ABSTRACT**

This study investigates the dynamic behavior of a vacuum packed particles torsional damper (VPPTD) filled with a 1:3 plastic (ABS – acrylonitrile butadiene styrene) and rubber (NBR – nitrile butadiene rubber) granulate mixture. Experimental results revealed that the system exhibits a symmetric hysteresis loop, with maximum torque increasing systematically with applied underpressure. The response was characterized by viscous damping, linear and nonlinear stiffness, and friction-related torque. The main novelty of the paper is the implementation of the physics-informed neural network (PINN) to accurately identify model parameters based on experimental data. In addition, to final parameter identification, a detailed analysis of the training process was conducted, revealing how the model progressively converged toward the experimental hysteresis loop. The identified model showed good agreement with measured data, and theoretical model. Parametric trends revealed a near-linear dependence of all model parameters on underpressure. These findings suggest that the model can be generalized by expressing parameters as functions of underpressure, paving the way for adaptive, pressure-aware control strategies.

**Keywords:** artificial intelligence, physics-informed neural network, hysteresis model, theoretical modelling, vacuum-packed particles torsional damper, adaptive damping.

## **INTRODUCTION**

Vibrations are an inherent phenomenon in almost all mechanical systems, arising from dynamic interactions between system components, external excitations, and environmental factors. If not properly controlled, excessive vibrations can significantly reduce the fatigue life of structural elements, accelerate the wear of components, and compromise operational reliability and safety [1–2]. For example, cyclic stresses induced by vibrations can cause the initiation and propagation of cracks in metal structures or delamination of composite materials [3]. Consequently, vibration damping has become a crucial aspect of engineering design, particularly in fields such as aerospace, automotive, civil engineering, and precision manufacturing [4–5]. An additional challenge arises from the fact that the excitations to which mechanical systems are subjected often vary in real time. Typical examples include changing road conditions that affect vehicle suspensions, fluctuating aerodynamic loads acting on the wings of the aircraft or variable forces encountered by robotic manipulators during interaction with dynamic environments [6–7]. In such scenarios, fixed damping solutions may not provide an optimal performance in all operating conditions.

Therefore, there is a growing interest in the development of adaptive structures and materials capable of adjusting their damping properties in response to changing external conditions. Such systems can improve vibration suppression in a wide range of applications, thereby enhancing structural durability and operational safety [8–11]. One of the intriguing solutions is vacuum packed particles (VPP), which is classified as a type of a smart materials. A core composed of granular material can alter its properties depending on the underpressure [9–11]. By adjusting this pressure,

it becomes possible to control the contact forces between individual grains, which in turn affects the damping characteristics of the system. In paper [12], the theoretical potential of using VPP dampers in blast-resistant seats was explored. Numerical simulations, based on prior research, confirmed the effectiveness of this technology in vibration attenuation in machinery [13]. VPP systems have also found applications in soft robotics. In [14], a shape-adaptive composite was presented, consisting of a granular core and a silicone shell embedded with channels containing liquid metal. Electromagnetic forces induce a change in the structure's shape, while the granular core stabilizes the newly formed geometry. This design was proposed as a gripper for industrial robots. Previous studies primarily focused on the behavior of VPP structures under compression, tension, and bending. The paper presented in [11] and [15] extended this research to include torsional loads, thereby contributing to a broader understanding of the properties of this innovative material technology. The proposed VPP system constitutes a more cost-effective, environmentally friendly, and operationally simpler alternative to magneto- or electrorheological fluids. The application of VPPs in rotary vibration dampers is a novel topic, and apart from the authors' earlier works [15], it has not been addressed in the international literature.

Experimental studies have shown that the behavior of the described VPP devices can be represented by either symmetric or asymmetric hysteresis loops. To analyze system behavior under conditions that cannot be replicated in laboratory experiments, or for the purpose of developing control algorithms, various theoretical models are proposed. These models effectively capture the operational principles of the devices. In the global literature, a range of mathematical models is utilized. The simulation process is always accompanied by the challenge of identifying the parameters of the selected model. Numerous established methods exist for determining the values of individual model components, ranging from the Monte Carlo method, through techniques such as the Levenberg-Marquardt algorithm, to genetic algorithms. Despite many years of advancement in hysteresis modeling and parameter identification techniques, there remains a continuous need for new solutions or novel combinations of existing methods to improve the efficiency and accuracy of theoretical simulation procedures. A particularly rapidly developing field of science is artificial intelligence and its applications in mechanical engineering. Artificial neural networks can be utilized to predict mechanical properties [16, 17] or to optimize [18] various mechanical systems.

The present article focuses precisely on this topic, exploring novel approaches to adaptive vibration damping based on underpressure-dependent devices presented in paper [15] and data-driven modeling techniques. The main novelty of this work lies in the use of a Physics-Informed Neural Network (PINN) for fast and efficient identification of the proposed theoretical model.

#### **EXPERIMENTAL INVESTIGATION**

The experimental tests were carried out on a specially developed prototype of a vacuum packed particles torsional damper (VPPTD). The damper and the test stand are shown in Figure 1 (1 – VPPTD; 2 – torque transducer; 3 – rotary encoder; 4 – electric motor; 5 – excitation mechanism; 6 - fixation point; 7 - hollow shaft). The device consists of several key components: an outer ring, an inner ring, two flexible sealing membranes creating a chamber. The chamber is filled with a granular mixture composed of ABS (acrylonitrile butadiene styrene) and NBR (nitrile butadiene rubber) 1:3 granulate (25\% ABS and 75\% NBR). During operation, an air is evacuated from the chamber through holes in the inner ring and the air is removed through a hollow shaft using a vacuum pump, which reduces the internal pressure. This underpressure causes the membranes to compress the granular core, altering its macroscopic structure and consequently changing the damper's mechanical response. The vacuum level is controlled dynamically by the pump. In this prototype, rotational input is applied through a clamping sleeve fixed to the outer ring, transferring motion through the deformable granular core to the inner ring. The excitation system was constructed as a dedicated mechanical setup consisting of an electric motor, an eccentric disc, a four-bar linkage, and an inverter. This arrangement made it possible to generate a harmonic excitation with a prescribed amplitude and an adjustable excitation frequency across a broad range. The measurement system included an encoder (HY38-1024HS), a torque transducer (Dataflex KTR 32/100), and a data acquisition card (Labjack T7), which together ensured precise recording of the angular displacement and torque during the experiments. Both the mechanical excitation subsystem and the measurement instrumentation were carefully calibrated and validated prior to the main experimental campaign. The calibration procedure guaranteed that the imposed excitation corresponded to the intended amplitude and frequency, while the validation confirmed the reliability of the recorded signals. As a result, the authors could be confident in the accuracy and reproducibility of the experimental data used for the subsequent modeling and identification process.

The VPPTD damper is designed as a system composed of an inner and an outer ring, which are interconnected by a flexible rubber membrane. This structural feature ensures the integrity and tightness of the device, but at the same time imposes mechanical constraints on its operational range. In particular, the presence of the membrane prevents a full relative rotation of the two rings. On the basis of preliminary examinations, the maximum allowable torsional angle was determined to be harmonic with amplitude 20°. Exceeding this limit could compromise the tightness of the system and potentially lead to its failure. To remain safely within this range and to avoid introducing undesired nonlinearities associated with extreme deformations of the membrane, the present investigation was carried out using a torsional amplitude of 10°. In previous work [15], a damper of identical construction was filled with a comparable type of granular material and studied under a range of excitation frequencies. The outcomes of that study indicated that, within the examined frequency range, the excitation frequency had no measurable influence on the global dynamic response of the damper. This observation

suggests that, for this type of device, the dissipation mechanisms are dominated primarily by the internal structure of the granular medium rather than by frequency-dependent effects. Building upon these findings, the current study adopts a fixed excitation frequency of 0.8 Hz. This value was intentionally selected in order to approximate quasi-static operating conditions, thereby allowing the focus to remain on the intrinsic energy dissipation characteristics of the VPPTD damper. By reducing the influence of inertial and rate-dependent effects, the study isolates the role of the granular medium and the membrane coupling in shaping the overall torque response of the device.

During the tests, the vacuum pressure inside the chamber was systematically varied in discrete steps, ranging from 0.01 MPa to 0.09 MPa. Throughout each test, the torque response of the damper was continuously measured as a function of both time and angular displacement of the outer ring. This allowed to collecting characteristics of the dynamic behaviour of the system under different vacuum levels, with particular attention to identifying the presence of hysteresis effects. The experimentally obtained torque – angle hysteresis curves for the full range of tested underpressures are presented in the Figure 2.

The curves exhibit two dominant features. First, at extreme angular displacements (near  $\pm 10^{\circ}$ ), there is a sudden change in torque curve for a relatively small change in angle, indicating a highly frictional behaviour during the changes of the direction rotation. Second, the intermediate portion of the curves displays a complex responses, suggesting a transition from a compliant to a stiffer regime as the angle increases. The maximum torque achieved varies significantly

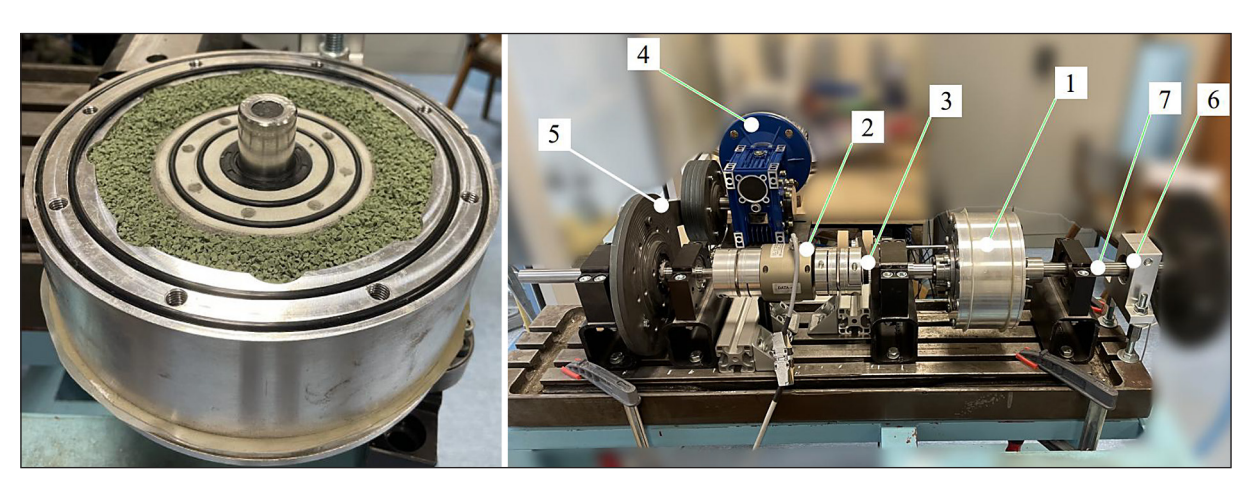


Figure 1. VPPTD prototype and test stand

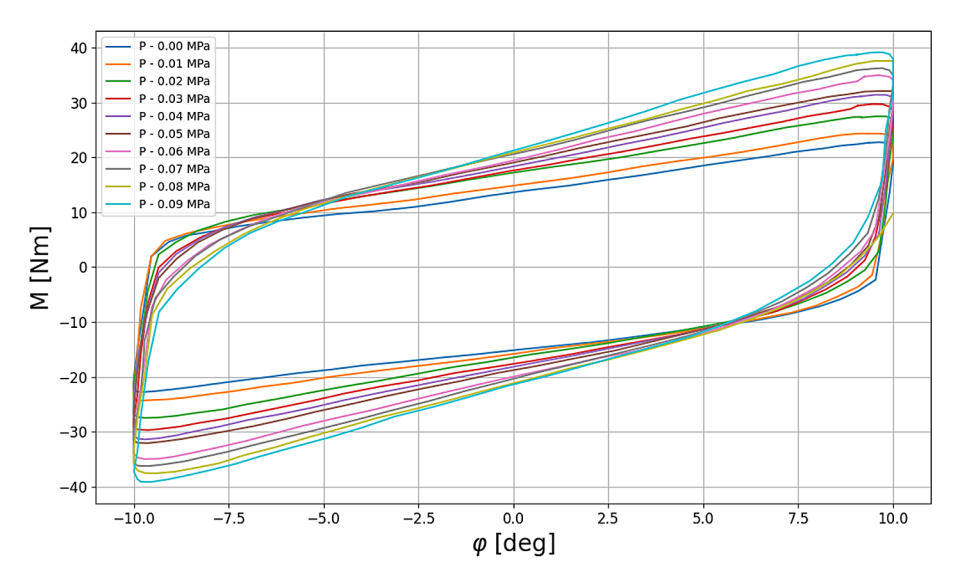


Figure 2. Experimental hysteresis loops for the various underpressures

with the applied underpressure: at the lowest pressure (0.01 MPa), the peak torque slightly exceeds 20 Nm, while at the highest pressure (0.09 MPa), it approaches 40 Nm. Despite this clear dependence of torque magnitude on underpressure, the overall shape of the hysteresis loops remains consistent across all tested conditions, indicating that the fundamental deformation mechanisms of the material are preserved regardless of the applied pressure. This consistent loop shape suggests stable material behaviour under varying operational conditions, with the primary effect of underpressure being a changes of stiffness and torque capacity. In study [15], analogous experiments were conducted on a system containing a 1:1 mixture of ABS-NBR granulate and pure rubber grains. A comparison of the results indicates that a higher proportion of plastic granulate leads to more highlights nonlinear behavior. The results obtained in this work, presented in Figure 2, not only confirm these observations but also extend the previous research by including mixtures that had not been investigated until now.

# HYSTERESIS MODELLING BY PHYSICS-INFORMED NEURAL NETWORK

In the field of intelligent materials and adaptive systems, accurately modeling the dynamic behavior of components is a key challenge, particularly when the response exhibits hysteresis. Hysteresis loops, similar to those observed in the experimental results obtained from the proposed

device, are a common feature in systems utilizing smart materials such as magnetorheological (MR) and electrorheological (ER) fluids, shape memory alloys (SMA), piezoelectric actuators, and elastomer-based composites [19]. These nonlinear, path-dependent behaviors arise from internal friction, phase transformations, or complex microstructural mechanisms, and they must be carefully captured for effective design and control.

To describe hysteretic behavior, a variety of mathematical models have been developed. One of the most widely used is the Bouc-Wen model [20]. The Bouc-Wen model offers great flexibility and can reproduce a wide variety of hysteresis shapes; however, its parameters can be difficult to interpret physically and require careful identification. Another popular class of models are Preisach models [21], which represent hysteresis as a superposition of many elementary relay operators with different thresholds. Preisach models are particularly suitable for capturing rate-independent hysteresis and have been extensively used in modeling magnetic materials and SMA. Their main drawback is computational complexity, especially in dynamic simulations. Dahl models [22] and LuGre friction models [23] are often employed in systems dominated by friction-induced hysteresis, such as robotic joints and brake systems. These models introduce internal state variables to capture dynamic friction effects and are well-suited for real-time control applications due to their relatively simple structure. Finally, Prandtl-Ishlinskii models [24] or Chaboche [25] offer a useful trade-off between flexibility and computational efficiency. They can accurately represent both rate-independent and rate-dependent hysteresis and allow for analytical inversion, which is particularly advantageous in control design.

Each of these modeling approaches has its own strengths and limitations. The choice of model depends on the specific characteristics of the hysteresis observed in the system, the intended application (e.g., simulation vs. control), and computational constraints. In the case of the VPPTD-based device analyzed in this study, the observed hysteresis behavior, characterized by a combination of nonlinear stiffness, viscous damping, and friction effects, lends itself naturally to modeling approaches that incorporate both ratedependent and path-dependent terms. The simple yet flexible model (Equation 1) adopted in this work reflects this philosophy and offers an effective compromise between physical interpretability and modeling accuracy.

$$M_{num} = c \frac{d\varphi}{dt} + k\varphi + k_2 \varphi^3 + M_s sign\left(\frac{d\varphi}{dt}\right) (1)$$

where:  $\varphi$  is an angle of rotation,  $\frac{d\varphi}{dt}$  is an angular velocity, c is a damping coefficient, k and  $k_2$  are a linear and nonlinear stiffness coefficient, respectively and  $M_c$  is a moment of a friction force.

The mathematical model described by the Equation 1 is used to predict the torque in mechanical systems where both linear and nonlinear effects play a role. The term  $c\frac{d\varphi}{dt}$  captures viscous phenomena, modeling the energy dissipation proportional to the angular velocity. The component  $k\varphi$  reflects the linear stiffness of the system, providing a restoring torque that is directly proportional to the angular displacement. The nonlinear stiffness term  $k_2 \varphi^3$  accounts for higher-order elastic effects that become significant at larger angular displacements, enabling the model to represent phenomena such as geometric nonlinearities or material nonlinear behavior. Additionally,  $M_s sign\left(\frac{d\varphi}{dt}\right)$  models friction, introducing a torque component that depends on the direction of motion, which is essential for accurately representing systems with dry friction. One of the key advantages of this model is its balance between simplicity and expressiveness. It can effectively capture complex dynamic behaviors while remaining computationally efficient and relatively easy to parameterize. This makes it highly suitable for real-time simulations,

control design, and parameter identification tasks in a wide range of engineering applications, from robotics and automotive systems to aerospace mechanisms and precision instruments. Furthermore, the model's modular structure allows for straightforward extensions or adaptations to match specific system characteristics, enhancing its versatility and practical utility.

## Identification of the hysteresis loop

The identification of model parameters describing hysteresis loops is a challenging task due to the nonlinear and path-dependent nature of hysteretic behavior. Accurate parameter estimation is crucial for reliable modeling and simulation of materials and systems exhibiting hysteresis. Various identification techniques, including optimization algorithms and data-driven methods, have been developed to address this problem. The complexity of the hysteresis phenomenon often requires balancing model accuracy with computational efficiency [26, 27, 28]. In recent years, genetic algorithms have emerged as one of the popular solutions for identifying parameters in hysteresis models. These algorithms are inspired by the principles of natural evolution and offer a robust approach to solving complex optimization problems. Genetic algorithms are particularly well-suited for dealing with the nonlinear and multidimensional nature of hysteresis parameter identification. Their ability to explore a wide solution space helps avoid local minima, leading to more accurate and reliable parameter estimation [29-31]. A notable drawback of genetic algorithms is their relatively high computational cost, especially for complex models or large datasets. Due to their stochastic nature and population-based search, they often require a large number of function evaluations, which can result in long processing times. Additionally, tuning the algorithm's parameters, such as population size, mutation rate, and crossover probability, can be challenging and significantly affect performance. In the literature, there are approaches that replace existing models with algorithms based on artificial intelligence. The paper [32] focuses on modeling the nonlinear behavior of particle dampers (PDs), which exhibit hysteresis under dynamic excitation. The authors propose using artificial neural networks to capture this complex phenomenon, addressing the issue of spectral bias that affects the learning of high-frequency components. To enhance model performance, the study combines Fourier feature embedding with transfer learning within a neural network framework. The main goal is to develop an accurate surrogate model capable of representing the PD's response across a wide frequency range. Another interesting approach was presented in paper [33] which focuses on improving the modeling of magnetic hysteresis using neural operator-based approaches. Traditional deep learning methods often struggle to generalize to previously unseen magnetic field inputs, which limits their practical application. To overcome this, the authors propose using neural operators, specifically DeepONet, Fourier neural operator (FNO), and wavelet neural operator (WNO), to learn the mapping between magnetic fields and material responses. The study also introduces a rate-independent variant of FNO to capture hysteresis behavior at different sampling rates. Numerical results show that these methods not only outperform conventional recurrent neural networks but also generalize well to novel magnetic field scenarios, offering a promising direction for the design and analysis of magnetic devices.

An analysis of the literature review reveals a lack of intermediate approaches, specifically, the application of neural networks to identify well-established and widely used phenomenological models. This study addresses that gap by proposing a solution in which the mathematical model (Equation 1) is identified using a physics-informed neural network (PINN), thereby bridging the existing void between purely data-driven and purely theoretical modeling methods.

## Physics - informed neural network

Physics-Informed neural networks (PINNs) represent a powerful class of machine learning methods that integrate physical laws directly into the training of neural networks, enabling them to learn solutions to complex dynamical systems in a data-efficient and physically consistent manner [34]. Unlike traditional neural networks, which rely solely on data to infer patterns, PINNs incorporate the governing equations of the system, such as differential equations, conservation laws, or constitutive relations, into the loss function used during training [35]. This approach ensures that the learned model not only fits the observed data but also respects the underlying physical principles, leading to improved generalization and interpretability. PINNs have been successfully applied to a wide range of problems, including fluid dynamics, solid mechanics, electromagnetics, and materials science [36–37].

One of their key advantages is the ability to model systems where experimental data may be sparse, noisy, or incomplete, by leveraging known physics to guide the learning process. Moreover, PINNs are well-suited for modeling complex nonlinear behaviors, such as hysteresis, as they can naturally incorporate both observed data and differential relations governing internal states. In this work, PINNs are employed as an effective tool for parameter identification in a hysteretic system, enabling the construction of a physically consistent and accurate model of the adaptive damping device.

The PINN architecture was deliberately simplified to focus exclusively on parameter identification. The network consisted of a single vector of four trainable parameters  $\theta = [c_{raw}, k_{raw}, k_{2raw}, M_{Sraw}]$  where each parameter was represented internally as an unconstrained real-valued variable  $p_{raw,j}$ . To ensure that the resulting physical parameters remained strictly positive, consistent with their physical interpretation, a *softplus* transformation was applied [38]:

$$p_j = \ln(1 + e^{p_{raw,j}}), j \in \{c, k, k_2, M_s\}$$
 (2)

Thus, the network performed unconstrained gradient-based optimization on  $p_{raw}$ , while the actual physical parameters  $p_j$  were guaranteed to remain positive.

In our implementation, the starting values of the trainable parameters were set close to zero and then perturbed by a small random offset, as defined in the code by the following initialization  $p^{(0)} = softplus^{-1}(max(+N(0,0.1), 10^{-6}))$ , where N(0,0.1) denotes a normally distributed random variable with zero mean and a standard deviation of 0.1, and the inverse softplus transformation was applied to ensure numerical stability and positivity of the parameters during training. The rationale for this choice was twofold. First, by initializing values close to zero, the optimization procedure was not biased toward any predefined solution, thereby allowing the parameters to be determined primarily by the experimental data. Second, the small stochastic perturbation ensured that the optimization process did not always start from identical initial conditions. This feature allowed us to verify the robustness of the procedure and to examine whether the final parameter values exhibit consistent trends with respect to

vacuum pressure, regardless of the specific initialization. As a result, the adopted initialization strategy provided both flexibility in the optimization and confidence that the observed dependencies of the identified parameters on vacuum pressure are inherent to the system and not artifacts of initialization. The loss function minimized during training was defined as:

$$Loss = \frac{1}{N} \sum_{i=1}^{N} |M_{num}(t_i) - M_{exp}(t_i)| +$$

$$+ \lambda \sum_{j=1}^{4} |p_j - p_{j,init}|$$
 (3)

where:  $M_{exp}(ti)$  is the experimentally measured torque, and  $\lambda$  is a regularization weight (set to 0.01). The first term corresponds to the mean absolute error (MAE) between predicted and experimental torque values.

The second term introduces an L1 regularization that penalizes deviations of the identified parameters from their initial estimates  $p_{j,init}$  thereby promoting stability and ensuring physically reasonable solutions. The training process was implemented using the Adam optimizer with a learning rate of 0.01. During backpropagation, gradients of the loss with respect to each raw parameter  $p_{raw,j}$  were computed by the following equations:

$$\frac{\partial Loss}{\partial p_{raw,j}} = \frac{\partial Loss}{\partial p_j} \cdot \frac{\partial p_j}{\partial p_{raw,j}} \tag{4}$$

$$\frac{\partial p_j}{\partial p_{raw,j}} = \sigma(p_{raw,j}) = \frac{1}{1 + e^{-p_{raw,j}}}$$
 (5)

The parameter identification was performed independently for each tested *P* which corresponds to the underpressure applied to the granular chamber of the VPPTD. The identification was conducted for pressure values ranging from 0.01 MPa to 0.09 MPa. For each case, the PINN was trained for 2000 epochs, and the identified parameter values were recorded. This approach provided a simple and powerful framework for identifying physically consistent parameters in hysteretic systems. The use of PINN ensured that the model strictly adhered to known physics while achieving excellent agreement with experimental data across varying operating conditions.

## THEORETICAL RESULTS

Based on the experimental data presented, a PINN was employed to identify the parameters of the theoretical model that describe the torqueangle behaviour of the ABS+NBR 1:3 material. In this study, each hysteresis loop corresponding to a single underpressure level consisted of approximately 1700 experimental data points. These points of angular displacement and torque were directly used as the training data for the identification procedure. With regard to collocation points, we acknowledge that in the standard physics-informed neural network framework, such points are introduced to enforce the residual of the governing differential equation across the domain. In the present work, however, we intentionally employed a simplified network structure, in which the model was formulated as a direct parametric regression rather than as a full PINN. Consequently, the training relied solely on the experimental data points, and no collocation points were incorporated. We recognize that this represents a departure from the classical PINN methodology. Nevertheless, this approach was adopted to focus the study on capturing the torque-angle relationship from experimental measurements and on revealing systematic dependencies of the identified parameters on underpressure. By incorporating both the physical principles governing the system and the measured data, the PINN enabled an accurate estimation of model parameters, capturing the observed nonlinear and hysteretic response. An example of the prediction of the resulting model is illustrated in Figure 3 which demonstrates good agreement between the theoretical and experimental curves.

Figure 3 compares the experimental torque response with the corresponding results obtained from the theoretical model identified using a PINN for the applied underpressure P = 0.09 MPa (for the last epoch of the training process). It demonstrates good general agreement between the two curves, particularly in capturing the characteristic hysteresis loop shape, the nonlinear stiffening at large angular displacements, and the general trend of torque variation with angle. Some minor discrepancies are observed near the transitions at extreme angles, where the sharp increase in torque is more pronounced in the experimental results. Nevertheless, the close correspondence between the curves confirms the effectiveness of the PINN-based parameter identification in

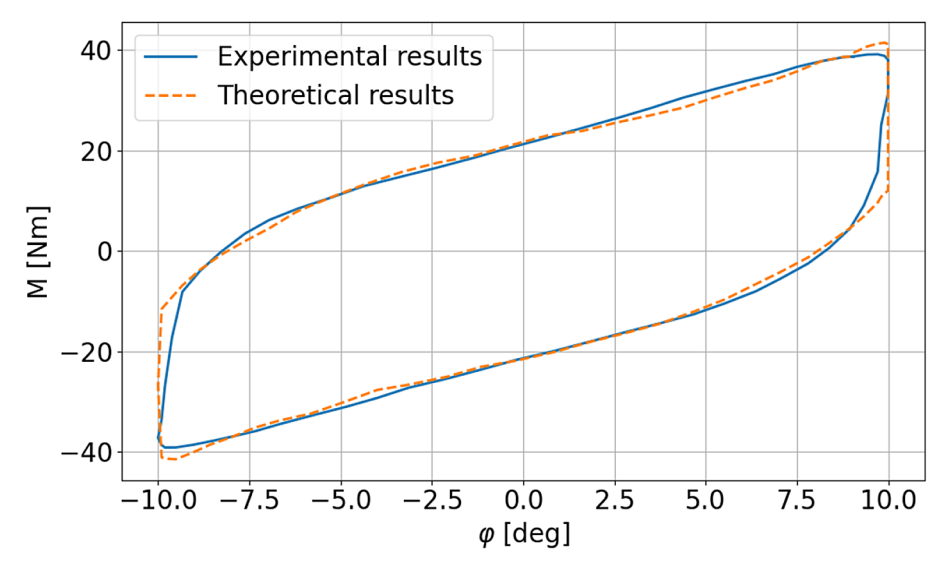


Figure 3. Comparison of the experimental and numerical results for the P = 0.09 MPa

accurately modeling the complex dynamic behavior of the composite material.

To provide a clearer understanding of the identification process, the evolution of the model fitting was illustrated by presenting hysteresis curves corresponding to intermediate sets of identified parameters at different stages of training. Specifically, the torque – angle curves obtained after 1, 400, 1000, and 2000 training epochs of

the PINN were plotted. This step-by-step visualisation highlights how the model progressively improves its representation of the experimental data as the training advances. Initially, the theoretical response shows significant deviations from the measured curve, but with increasing epochs, the fit becomes progressively more accurate, eventually capturing both the overall shape and the detailed features of the experimental hysteresis

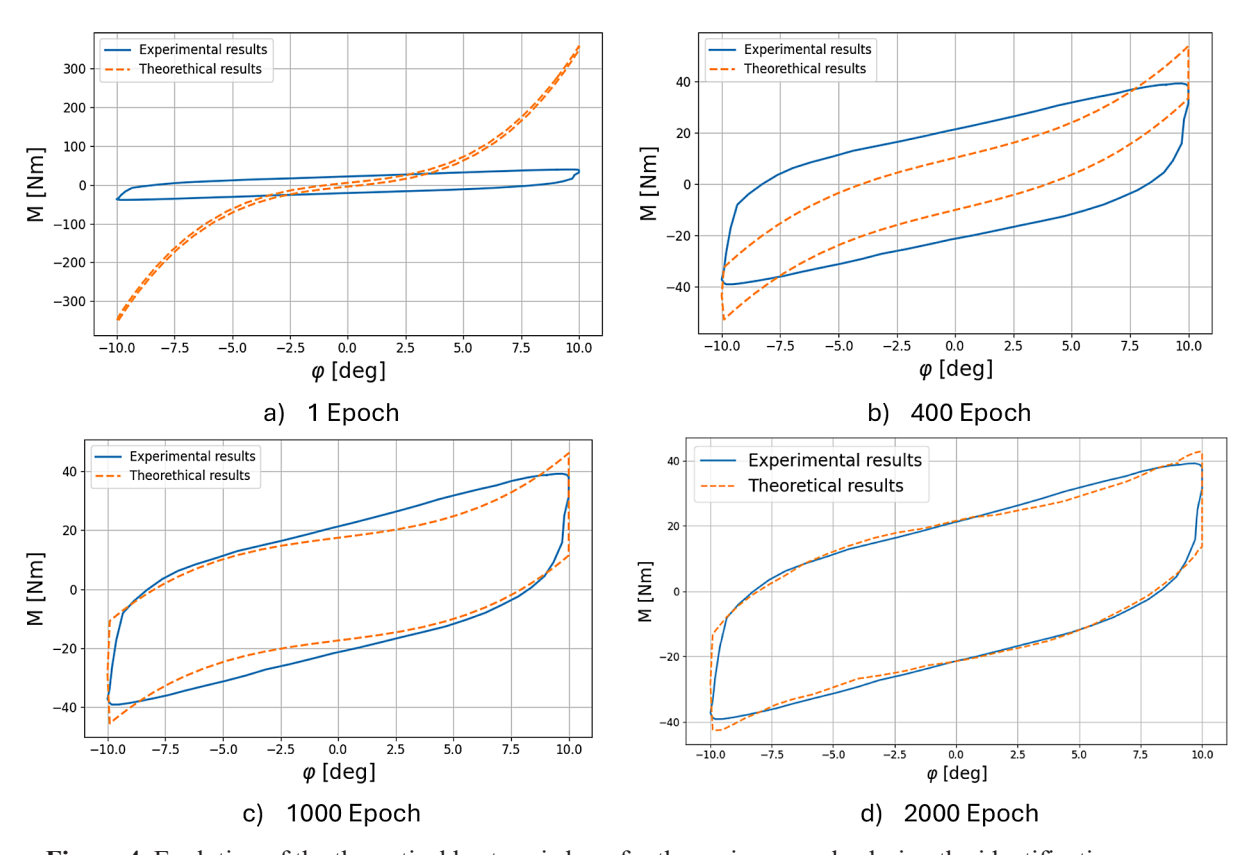


Figure 4. Evolution of the theoretical hysteresis loop for the various epochs during the identification process

loop. This approach provides valuable information on the learning dynamics of the PINN and the convergence of the parameter identification process (Figure 4).

In Figure 5, the evolution of the identified model parameters - specifically the damping coefficient c, the linear stiffness k, the nonlinear stiffness k, and the friction torque  $M_{\rm s}$  – is presented as a function of training epochs. This visualisation provides insight into the dynamics of the parameter optimisation process performed by the Physics-Informed Neural Network. Initially, the parameters exhibit significant fluctuations as the network explores the parameter space to minimise the loss function. As training progresses, the parameter values gradually stabilise, indicating convergence toward an optimal set that best represents the experimental data. The plots clearly demonstrate how the PINN balances the contributions of different physical effects (damping, stiffness, and friction) throughout training, ultimately resulting in a physically consistent and accurate model of the dynamic behaviour of the system.

The presented plots illustrate the evolution of the model parameters over the course of 2000 training epochs. Each parameter exhibits a distinct convergence behavior, providing valuable insights into the learning dynamics of the PINN-based identification process. The damping coefficient c remains close to zero up to approximately epoch 1000, after which it rapidly increases and

continues to grow, reaching a value of about 7.5 Nm·s by epoch 2000. This suggests that damping was initially underrepresented in the model but became more significant in the later stages of training. The linear stiffness k shows a steep initial decrease from around 5.5  $\frac{\text{Nm}}{\text{deg}}$  to approximately 1.8  $\frac{\text{Nm}}{\text{deg}}$  within the first 500 epochs, followed by a gradual stabilization with a slight upward trend toward 2.0  $\frac{\text{Nm}}{\text{deg}}$  by epoch 2000. Similarly, the nonlinear stiffness  $k_2$  rapidly decreases from about 0.14  $\frac{Nm}{deg^3}$  to below 0.02  $\frac{Nm}{deg^3}$  during the early epochs and remains relatively stable thereafter, indicating that the network quickly adjusted this parameter to reflect the material's weak nonlinear elastic response. The friction torque M<sub>s</sub> exhibits a distinct growth phase, increasing steadily from approximately 5 Nm to a peak value of about 17.5 Nm at epoch 1100, followed by a slight decline to around 14 Nm by the end of training. This behavior suggests that the network initially overcompensated for friction effects and subsequently refined the estimate for better overall model accuracy. These

The loss function used in the Physics-Informed Neural Network training process quantifies the discrepancy between the model predictions and the experimental data, guiding the

parameter trajectories highlight how the PINN

progressively balances the different physical con-

tributions in the model to achieve an accurate rep-

resentation of the observed hysteresis behavior.

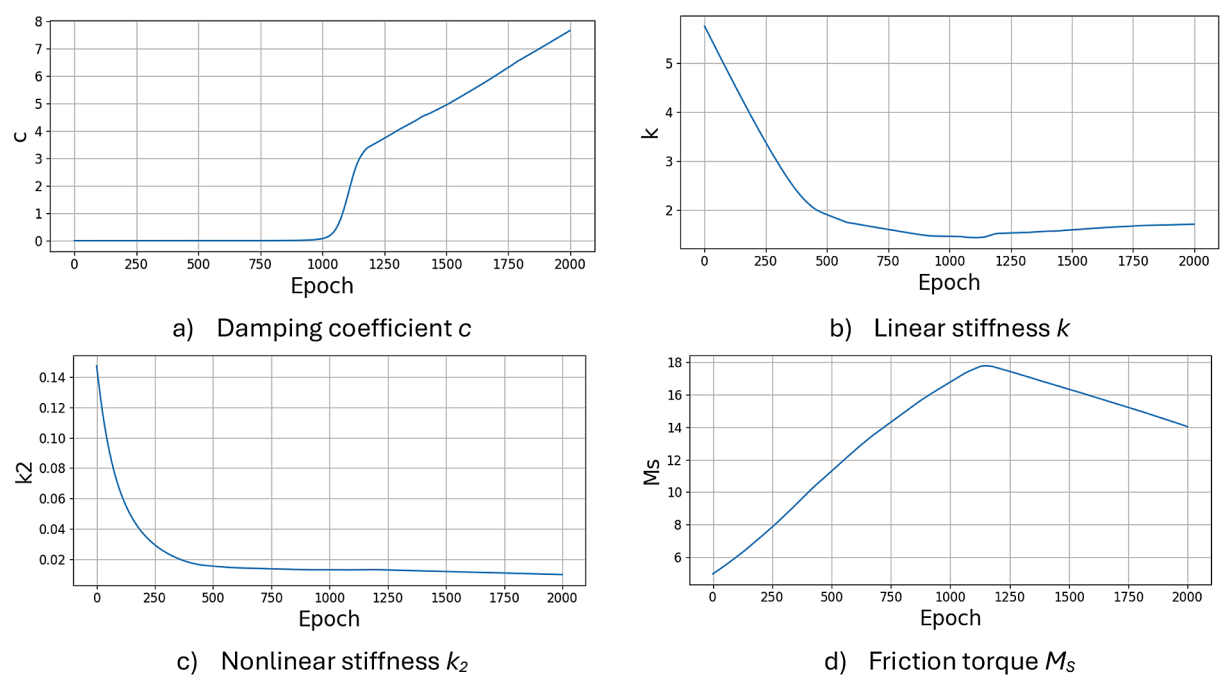


Figure 5. Evolution of the model parameters during the identification process

optimization of model parameters toward an accurate representation of the system's behavior. It typically combines terms reflecting both data fidelity and adherence to the underlying physical laws. In Figure 6, the loss function value over the course of training epochs is presented and illustrating how the model progressively reduces the error as the training proceeds. A decreasing loss curve indicates effective learning, while its final flattening suggests that the network has reached an optimal or near-optimal set of parameters corresponding to a well-fitted theoretical model.

In an analogous manner, the parameter identification process using the PINN was conducted for the remaining cases corresponding to different levels of applied underpressure. For each underpressure, the network was trained to optimise the model parameters to accurately capture the distinct torque-angle response observed experimentally. The comparative results of these identification processes are presented in the following, illustrating the effectiveness and consistency of the proposed approach across the full range of under conditions tested. These results also provide valuable information on how the dynamic behaviour of the material and the corresponding model parameters evolve as a function of the applied underpressure (Figure 7).

The general results demonstrate that the identification process was successful in all cases tested. The error between the experimentally measured torque—angle curves and the corresponding numerical predictions obtained from the PINN is consistently small for each level of applied underpressure. This indicates that the identified models accurately capture the key features of the response of the material. Moreover, the proposed PINN-based

identification method has proven to be robust, effective, and versatile, enabling the reliable estimation of physically meaningful parameters even in the presence of nonlinearities and hysteresis effects. In general, the approach offers a promising and practical tool for modelling complex dynamic systems based on experimental data. It should also be emphasized that the proposed model (Equation 1), combined with PINN-based identification, serves as an effective alternative to the phenomenological Bouc—Wen model used in paper [15], where the hysteresis loops exhibited similar characteristics and reached comparable values.

In Figure 8, the values of the identified model parameters are presented for different levels of applied underpressure. This visualisation provides a clear overview of how the key physical properties of the ABS+NBR 1:3 material changes as a function of pressure. By analysing these trends, valuable information can be gained about the influence of pressure on the damping characteristics, stiffness (both linear and non-linear), and friction behaviour of the material. The presented results further confirm the consistency and reliability of the parameter identification process in the full range of tested conditions.

The presented set of figures illustrates how the identified model parameters c, k,  $k_2$ , and  $M_s$  vary as a function of the applied underpressure P. Across all parameters, a clear trend of increasing values with rising vacuum pressure is observed, although some fluctuations are present. For the damping coefficient c, values range from approximately  $6.7 \frac{Nm \cdot s}{deg}$  at P = 0.01 MPa to a maximum of about  $8.3 \frac{Nm \cdot s}{deg}$  at P = 0.07 MPa, with an overall increasing tendency across the pressure range.

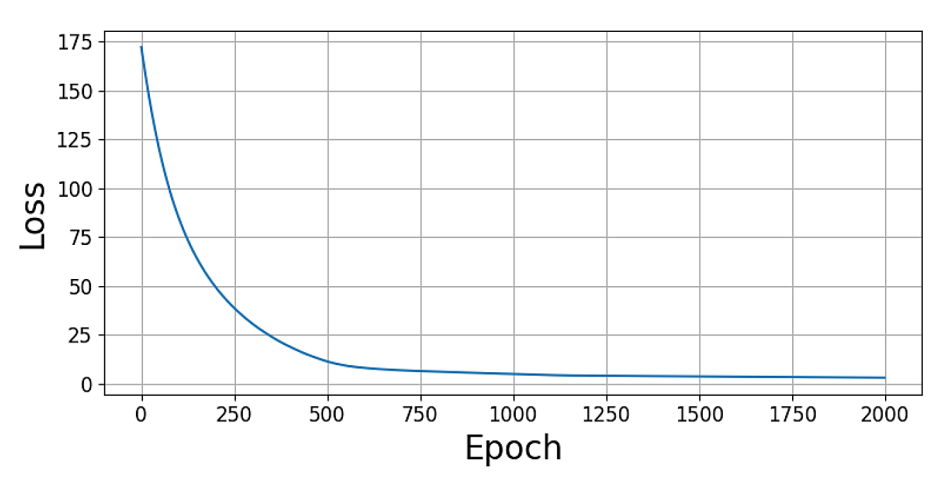
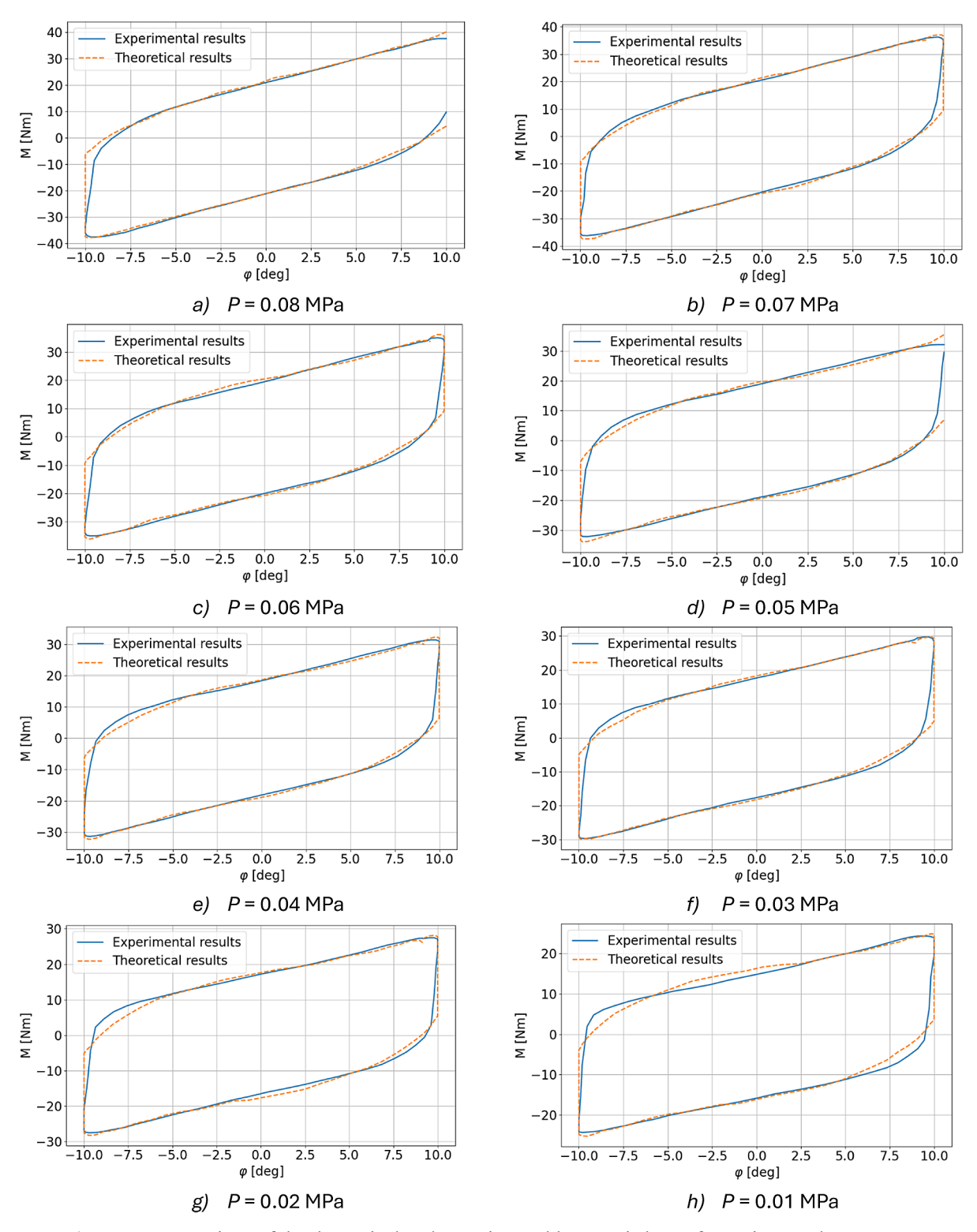


Figure 6. Changes of the loss function during the identification process

Nm deg



**Figure 7.** Comparison of the theoretical and experimental hysteresis loops for various underpressures (from 0.08 to 0.01 MPa)

The linear stiffness k also increases, starting from around 0.65  $\frac{Nm}{deg}$  at P=0.01 MPa and reaching up to approximately 1.65  $\frac{Nm}{deg}$  at P=0.08 MPa. The nonlinear stiffness  $k_2$  follows a similar trend, with values ranging from about 0.0055  $\frac{Nm}{deg^3}$  at P=0.08 MPa.

= 0.08 MPa to a peak of approximately 0.0145  $\frac{\text{Nm}}{\text{deg}^3}$  at P = 0.09 MPa. Finally, the friction torque  $M_s$  shows a strong positive correlation with vacuum pressure, increasing from roughly 9.5 Nm at P = 0.01 MPa to over 15 Nm at P = 0.08 MPa.

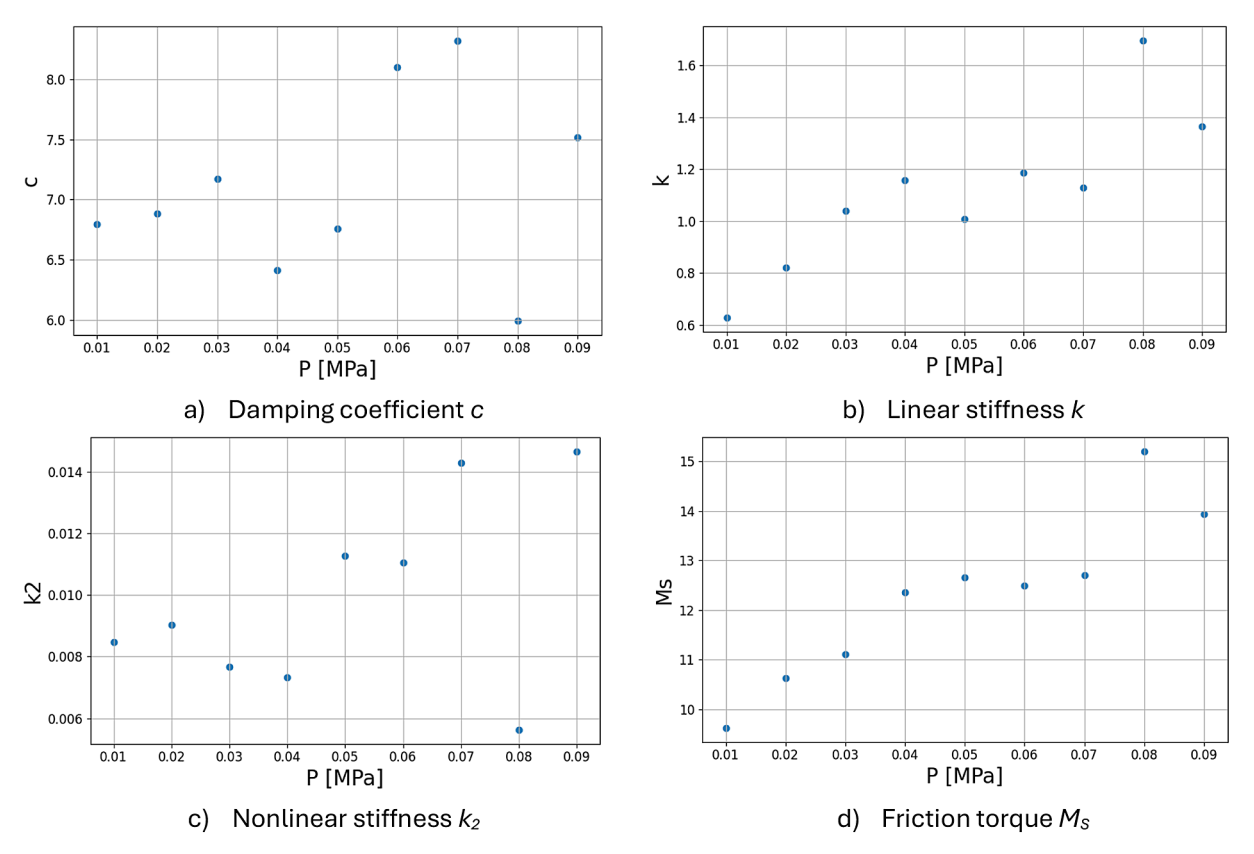


Figure 8. Identified model parameters for various underpessures

Despite minor nonlinearities and local variations, the general upward trend of all four parameters with increasing underpressure suggests that the dynamic behavior of the ABS+NBR 1:3 grains mixture becomes progressively stiffer and more dissipative as underpressure rises. These observed relationships indicate that the parameters could potentially be expressed as functions of underpressure, enabling the generalization of the theoretical model to predict the system's behavior continuously across different operating conditions. This would further enhance the model's applicability in practical engineering contexts.

In the subsequent analyses, a more detailed investigation was conducted to examine the evolution of each identified model parameter throughout the training process, across all tested levels of underpressure. By analyzing how these parameters evolved over the course of training epochs for each pressure value, it was possible to gain deeper insights into the learning dynamics of the PINN and the stability of the identification process. This approach also allowed for an assessment of how consistently and robustly the network adapted to different physical conditions, providing a comprehensive understanding of how underpressure influences not only the

final parameter values, but also their convergence behavior during training. The following figures present the results of these analyses.

Figure 9 shows the changes of the c as a function of training epochs for each tested level of underpressure P, ranging from 0.01 MPa to 0.09 MPa. Across all cases, the parameter c remains near zero during the initial phase of training (up to approximately 1000 epochs), indicating that the network initially prioritises fitting other aspects of the model. After this point, a rapid increase in c is observed for all pressure levels, followed by a more gradual growth phase. This behaviour suggests that the contribution of damping becomes significant only after the primary structural parameters are roughly established. Despite slight variations in the rate of increase, the general trends for different pressure levels are similar. In particular, higher final c values are consistently associated with higher underpressures. The consistency of the curves also indicates a stable and robust convergence behaviour of the network under all conditions (Figure 10).

In all cases, k exhibits a characteristic convergence pattern: it starts with a relatively high initial value (around 5.5–6.0) and undergoes a steep decline during the first 500–600 epochs, indicating

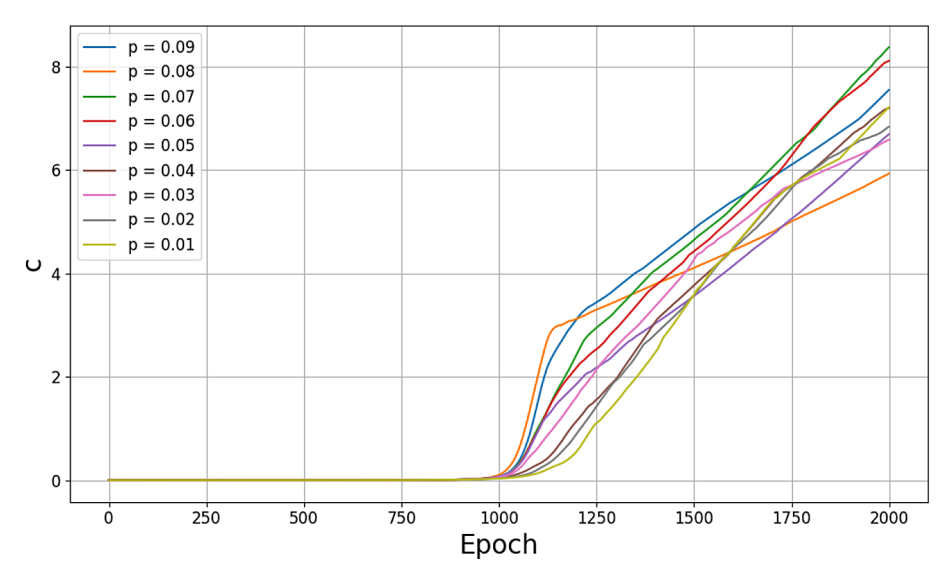


Figure 9. Evolution of the damping coefficient c during the identification process for various underpressures

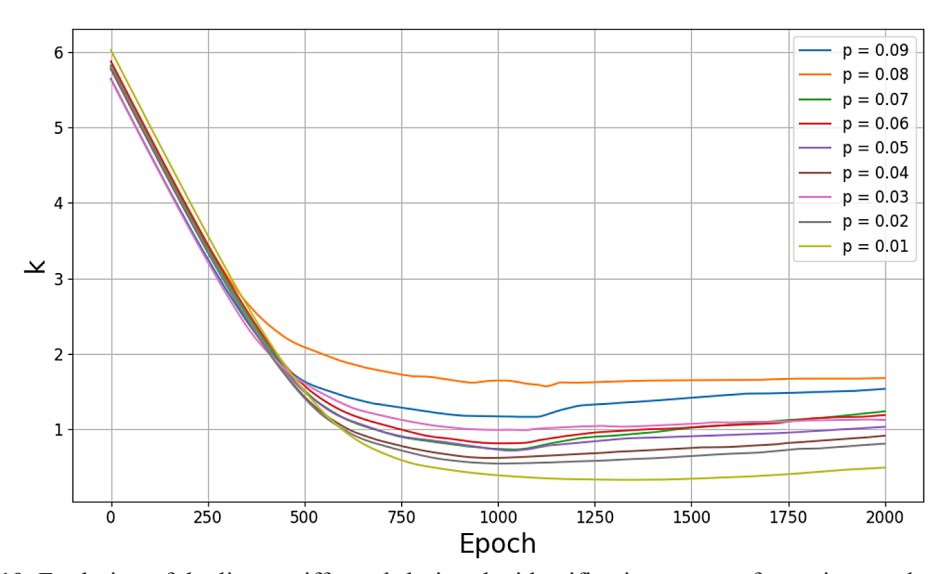


Figure 10. Evolution of the linear stiffness k during the identification process for various underpressures

that the network quickly adjusts this parameter to better fit the experimental data. After this initial drop, the parameter gradually stabilises, with slight differences emerging between the curves corresponding to different vacuum pressures. In particular, higher underpressures tend to be associated with higher final values of k. The relatively smooth and monotonic evolution of the parameter across all pressure levels indicates a stable and consistent learning dynamics. The slight upward adjustments seen after 1000 epochs, particularly at higher pressures, suggest that the network continues to refine the stiffness contribution to optimize the overall model fit during the later training stages (Figure 11).

Across all cases, the parameter  $k_2$  exhibits a very consistent and characteristic convergence pattern. It starts from relatively high initial values, between approximately 0.08 and 0.35, and undergoes a rapid and steep decrease within the first 500 epochs. After this initial phase, the curves gradually flatten out and stabilize near small positive values close to zero. The convergence behavior is highly similar across different underpressure levels, with only minor variations in the final values. This suggests that while the nonlinear stiffness component plays an important role during the early stages of training, likely compensating initially for the lack of tuning in other parameters, its relative contribution

becomes less dominant as the model converges. The consistent flattening of the curves indicates that the network robustly identifies a weak but non-negligible nonlinear stiffness component across all tested underpressures. Notably, there is no clear monotonic trend of final  $k_2$  values with increasing underpressure, in contrast to the linear stiffness k and damping c. This suggests that the influence of underpressure on the nonlinear stiffness of the system is either weak or more complex than a simple linear relationship.

This Figure 12 presents the evolution of the friction torque parameter. An initial steady increase in  $M_s$  up to approximately 1000 epochs, followed by a gradual decrease during the later stages of training. Initially,  $M_s$  grows linearly from about 5 to 6 Nm to its peak values. The maximum values of  $M_{\rm s}$  vary depending on the pressure level: at higher pressures (e.g. p = 0.08 MPa and p = 0.09 MPa. The observed trend confirms that the friction torque parameter  $M_c$  is strongly influenced by the underpressure, with higher P consistently leading to higher final values of  $M_{\odot}$ . The initial rise and subsequent fine-tuning phase reflect the network's effort to accurately capture the friction-related hysteresis behaviour of the system. In general, the stability and systematic variation of  $M_{\rm s}$  at different pressures further reinforce the conclusion that underpressure plays a significant and predictable role in shaping the frictional dynamics of the system (Figure 13). In all cases, the loss exhibits a very similar and well-behaved convergence pattern. Initially, the loss values are relatively high, exceeding 150 for several cases, but decrease rapidly within the first 500 epochs, reflecting the network's ability to quickly reduce the discrepancies between the predictions of the model and the experimental data. Beyond approximately 750–1000 epochs, the loss curves flatten and approach small values (below 10), indicating that the network has effectively converged to an optimal or near-optimal solution for all tested pressures. The final loss values in all cases are very similar, with no significant differences attributable to underpressure, demonstrating the robustness and stability of the identification process.

In the identification process it was observed that not all model parameters exhibit clear convergence during training. This applies in particular to the parameters c (viscous damping) and Ms (static friction torque), whose values do not stabilize around a single constant number but may show increasing, decreasing, or oscillatory behavior across epochs. This phenomenon arises from the fact that there exist multiple combinations of these two parameters that lead to almost identical agreement between the theoretical torque and the experimental torque. However, the lack of strict parameter convergence does not pose a significant problem for the identification process. The primary goal of the procedure is to determine parameter values that ensure the theoretical torque curve matches the experimental one as closely as possible. From this perspective, it is not essential for each parameter to converge individually; what matters is that the parameter set as a whole enables faithful reproduction of the observed response. Moreover, even though c and Ms do not converge in a strict numerical sense

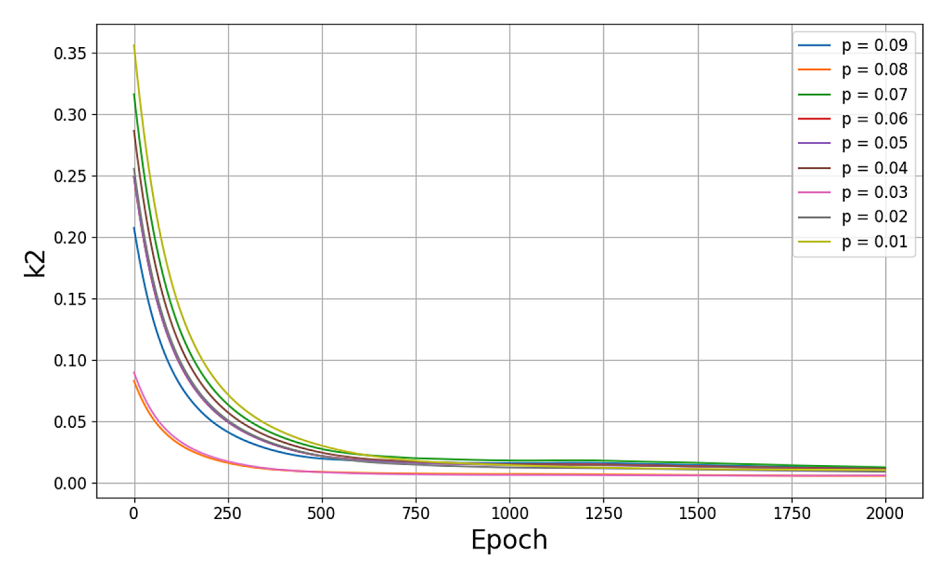


Figure 11. Evolution of the nonlinear stiffness  $k_2$  during the identification process for various underpressures

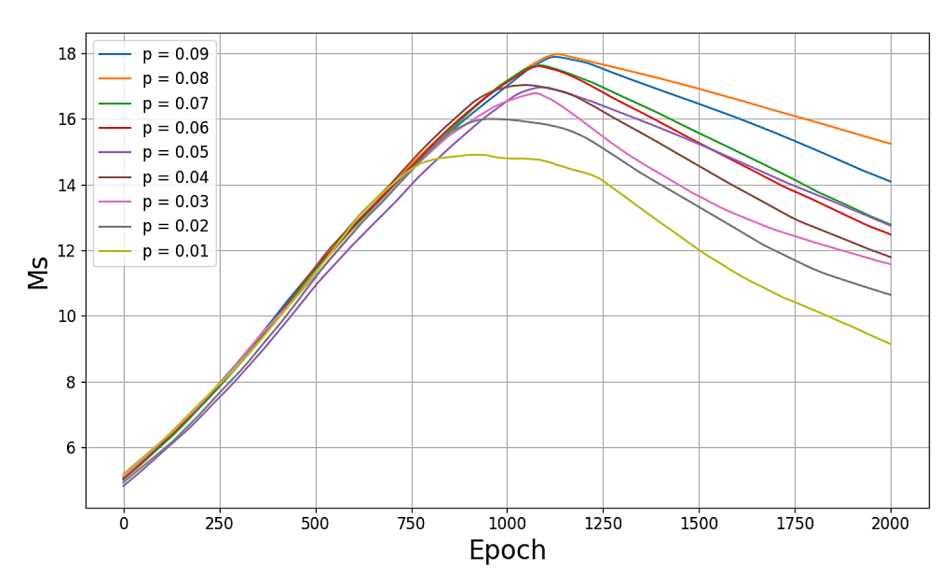


Figure 12. Evolution of the friction torque  $M_s$  during the identification process for various underpressures

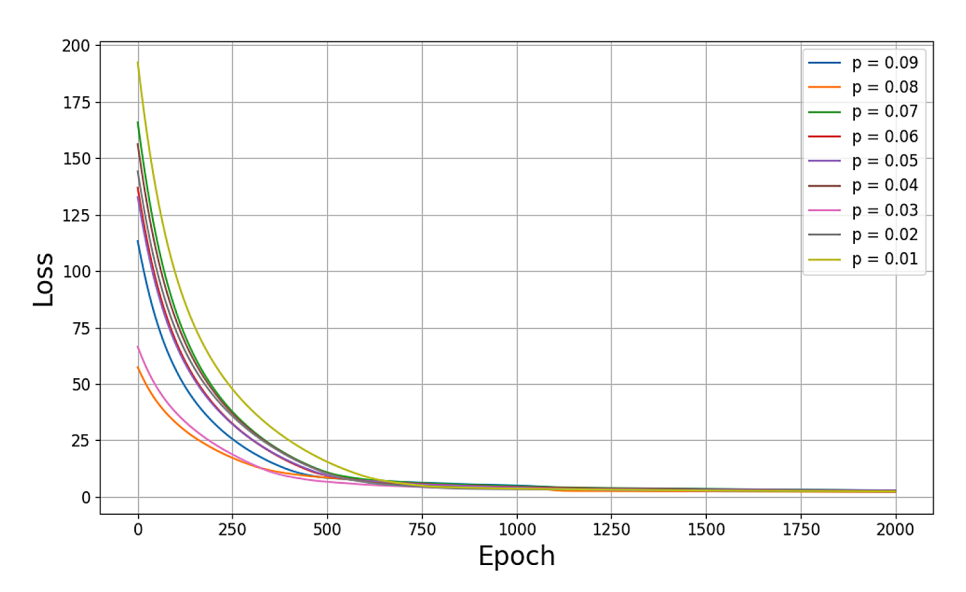


Figure 13. Evolution of the loss function Loss during the identification process for various underpressures

during training, their final identified values still exhibit a meaningful physical characteristic: they show a dependency on the applied underpressure. This indicates that, while these parameters may partially compensate for each other during optimization, their final values nevertheless carry information about how the operating conditions influence the behavior of the system.

In summary, the absence of full convergence in some parameters does not diminish the quality of the model identification. The model successfully fulfills its main objective, accurately reproducing the torque response, and highlights relevant physical trends through the pressure dependence of the identified parameters.

## **CONCLUSIONS**

In this paper, the dynamic behaviour of a vacuum packed particles torsional damper based on a 1:3 ABS-NBR granulate mixture was systematically investigated. Based on experimentally captured characteristics, an appropriate mathematical model was proposed, consisting of four key parameters: the viscous damping coefficient c, the linear stiffness k, the nonlinear stiffness  $k_2$ , and the friction torque  $M_s$ . The main novelty of this article is the implementation of an artificial intelligence algorithm within the numerical simulation process. To accurately identify parameters, a physics-informed neural network approach was employed,

ensuring that the theoretical torque model was optimally fitted to the experimentally obtained hysteresis curves. In addition to final parameter identification, a detailed analysis of the evolution of the theoretical hysteresis loop during the PINN training process was conducted. This analysis revealed how the shape of the model-based hysteresis loop progressively converged toward the experimental one over successive training epochs. Furthermore, the identification dynamics were studied in detaila. It was observed that in the early stages of training, the PINN primarily adjusted the components related to friction torque and stiffness in order to match the gross shape of the hysteresis loop. Only in later epochs did the network begin to increase the contribution of the viscous damping and linear stiffness terms to refine the loop's smoothness and accuracy. At convergence, it was also observed that the nonlinear stiffness component had the smallest influence on the final loop shape compared to the other three model terms. Overall, the final identified hysteresis loops showed very close agreement with the experimental results, validating both the accuracy of the model and the effectiveness of the PINN-based identification method. Parametric analysis demonstrated that all identified parameters systematically increased with underpressure and exhibited an approximately linear trend. This observation suggests that the proposed model could be generalised by explicitly expressing the parameters as functions of vacuum pressure, thereby enhancing its predictive capacity.

Future work will focus on extending the proposed modelling approach by explicitly formulating the model parameters as continuous functions of underpressure, enabling real-time adaptive control of the VPPTD system. In addition, further studies will explore the application of more advanced hysteresis modelling techniques and the integration of PINN-based models into closed-loop control architectures. Experimental validation will also be performed under dynamic operating conditions and varying excitation profiles to assess the practical performance and robustness of the system in real-world applications.

## REFERENCES

 Lu Z., et al. Nonlinear dissipative devices in structural vibration control: A review, Journal of Sound and Vibration. 2018; 423(9). https://doi.org/10.1016/j. jsv.2018.02.052

- Saaed TE, Nikolakopoulos G, Jonasson J-E, Hedlund H, A state-of-the-art review of structural control systems. Journal of Vibration and Control. 2013; 21(5). https://doi.org/10.1177/1077546313478294
- 3. Zhang YW, Zhang H, Hou S, Xu KF, Chen LQ, Vibration suppression of composite laminated plate with nonlinear energy sink, Acta Astronautica, 2016; 123. https://doi.org/10.1016/j.actaastro.2016.02.021
- Zurawski M, Zalewski R, Chilinski B, Concept of an adaptive-tuned particles impact damper, Journal of Theoretical and Applied Mechanics. 2020; 58(3). https://doi.org/10.15632/JTAM-PL/122431
- Żurawski M, Zalewski R, Experimental studies on adaptive-passive symmetrical granular damper operation, Materials. 2022; 15(17). https://doi. org/10.3390/ma15176170
- Grzesikiewicz W, Makowski M, Semi-active system of vehicle vibration damping, Applied Sciences Switzerland, 2021; 11(10). https://doi.org/10.3390/app11104577
- Abdel-Rohman M, John MJ, Control of wind-induced nonlinear oscillations in suspension bridges using multiple semi-active tuned mass dampers. Journal of Vibration and Control. 2006; 12(9). https://doi.org/10.1177/1077546306069035
- Żurawski M, Graczykowski C, Zalewski R, The prototype, mathematical model, sensitivity analysis and preliminary control strategy for Adaptive Tuned Particle Impact Damper, Journal of Sound and Vibration. 2023; 564. https://doi.org/10.1016/j. jsv.2023.117799
- Rodak D, Zalewski R, Innovative controllable torsional damper based on vacuum packed particles, Materials. 2020; 13(19). https://doi.org/10.3390/ma13194356
- Bartkowski P, Zalewski R, A concept of smart multiaxial impact damper made of vacuum packed particles, MATEC Web of Conferences. 2018; 157. https://doi.org/10.1051/matecconf/201815705001
- Żurawski M, Chiliński B, Zalewski R, A novel method for changing the dynamics of slender elements using sponge particles structures, Materials. 2020; 13(21). https://doi.org/10.3390/ma13214874
- Zalewski R, Rodak D, Preliminary study of the Vacuum Packed Particles torsional damper, Journal of Theoretical and Applied Mechanics. 2021; 59(1). https://doi.org/10.15632/jtam-pl/130633
- 13. Zalewski R, Chodkiewicz P, Semi-active linear vacuum packed particles damper, Journal of Theoretical and Applied Mechanics. 2016; 54(1). https://doi.org/10.15632/jtam-pl.54.1.311
- 14. Jiles D, Introduction to Magnetism and Magnetic Material. 2015. https://doi.org/10.1201/b18948
- 15. Rodak D, Żurawski M, Pyrz M, Zalewski R, Modelling and identification of hysteresis of Vacuum

- Packed Particles Torsional Damper, Journal of Sound and Vibration. 2025; 616. https://doi.org/10.1016/j.jsv.2025.119203
- 16. Al-Wswasi M, Al-Khaleeli WA, Aufy SA. Implement the artificial neural network concept for predicting the mechanical properties of printed polylactic acid parts. Advances in Science and Technology Research Journal. 2025; 19(5): 73–83. https://doi.org/10.12913/22998624/201463
- 17. Al-Bdairy AMJ, Ghazi SK., Abed AH. Prediction of the mechanical properties for 3D printed rapid prototypes based on artificial neural network. Advances in Science and Technology Research Journal. 2025; 19(3): 96–107. https://doi.org/10.12913/22998624/197405
- 18. Grzeszczyk MK. Optimization of machine learning process using parallel computing. Advances in Science and Technology Research Journal. 2018; 12(4): 81–7. https://doi.org/10.12913/22998624/100341
- 19. Lagoudas DC. Shape memory alloys: modeling and engineering applications, Springer. 2008; https://doi.org/10.1007/978-0-387-47685-8
- Wen YK. Method for random vibration of hysteretic systems. Journal of Engineering Mechanics Division. 1976; 102(2). https://doi.org/10.1061/ JMCEA3.0002106
- 21. Mayergoyz ID. Mathematical Models of Hysteresis, Springer. 1991. https://doi.org/10.1007/978-1-4612-3028-1
- 22. Dahl PR. A solid friction model, The Aerospace Corporation, Technical Report. 1968; 18.
- 23. Canudas de Wit C, Olsson H, Åström KJ, Lischinsky P. A new model for control of systems with friction, IEEE Transactions on Automatic Control. 1995; 40(3). https://doi.org/10.1109/9.376053
- 24. Rakotondrabe M. Classical and Prandtl–Ishlinskii hysteresis modeling and inverse control of a three-axis piezoelectric micromanipulator, IEEE Transactions on Control Systems Technology. 2010; 18. https://hal.science/hal-00799726v1
- 25. Wójcik M, Gontarz A, Skrzat A, Winiarski G. Computational methods of the identification of Chaboche isotropic-kinematic hardening model parameters derived from the cyclic loading tests. Advances in Science and Technology Research Journal. 2024; 18(1): 61–75. https://doi.org/10.12913/22998624/175930
- 26. Hoffmann K-H, Sprekels J, A Visintin, Identification of hysteresis loops, Journal of Computational Physics, 1988; 78(1): 215–230. https://doi.org/10.1016/0021-9991(88)90045-9
- 27. Ruina ZHU, et al. Modeling and parameter identification of rate-dependent hysteresis behavior based on modified-generalized Prandtl–Ishlinskii model. *Smart Materials and Structures*, 2024; 33(7). https://doi.org/10.1088/1361-665X/ad4d38

- 28. Zhou M, Dai Z, Zhou Z, Liu X, Cao T, Li Z. Modeling, identification, and high-speed compensation study of dynamic hysteresis nonlinearity for piezoelectric actuator. *Journal of Intelligent Material Systems and Structures*. 2024; 35(9): 822–844. https://doi.org/10.1177/1045389X231225492
- 29. Chwastek K, Szczyglowski J. Identification of a hysteresis model parameters with genetic algorithms, Mathematics and Computers in Simulation, 2006; 71(3): 206–211. https://doi.org/10.1016/j.matcom.2006.01.002
- 30. Wilson PR, Ross JN and Brown AD. Optimizing the Jiles-Atherton model of hysteresis by a genetic algorithm, *IEEE Transactions on Magnetics*. 2001; 37(2): 989–993. https://doi.org/10.1109/20.917182
- 31. Kucuk I. Prediction of hysteresis loop in magnetic cores using neural network and genetic algorithm. Journal of Magnetism and Magnetic Materials. 2006; 305(2): 423–427. https://doi.org/10.1016/j.jmmm.2006.01.137
- 32. Ye X, Ni Y-Q, Ao WK, Yuan L. Modeling of the hysteretic behavior of nonlinear particle damping by Fourier neural network with transfer learning, Mechanical Systems and Signal Processing. 2024; 208. https://doi.org/10.1016/j.ymssp.2023.111006
- Chandra A, Daniels B, Curti M, Tiels K and Lomonova EA. Magnetic hysteresis modeling with neural operators, *IEEE Transactions on Magnetics*. 2025; 61(1): 1–11. https://doi.org/10.1109/TMAG.2024.3496695
- 34. Raissi M, Perdikaris P, Karniadakis GE. Physics-informed neural networks: A deep learning framework for solving forward and inverse problems involving nonlinear partial differential equations, Journal of Computational Physics. 2019; 378. https://doi.org/10.1016/j.jcp.2018.10.045
- Karniadakis GE., Kevrekidis IG, Lu L, Perdikaris P, Wang S, Yang L. Physics-informed machine learning. Nature Reviews Physics. 2021; 3. https://doi. org/10.1038/s42254-021-00314-5
- 36. Cuomo S, Di Cola VS., Giampaolo F, Rozza G, Raissi M, Piccialli F, Scientific machine learning through physics-informed neural networks: Where we are and what's next, Journal of Scientific Computing. 2022; 92. https://doi.org/10.1007/ s10915-022-01939-z
- Pang, G., Lu, L., Karniadakis, G. E. fPINNs: Fractional physics-informed neural networks, SIAM Journal on Scientific Computing. 2019; 41(4). https://doi.org/10.1137/18M1229845
- 38. Sun K, Yu J, Zhang L, Dong Z. A Convolutional neural network model based on improved soft plus activation function, Advances in Intelligent Systems and Computing. 2020; 1017. https://doi.org/10.1007/978-3-030-25128-4\_164